Implications of TCO Topography on Intermediate Reflector Design for a-Si/μc-Si Tandem Solar Cells—Experiments and Rigorous Optical Simulations

Simon Kirner, Martin Hammerschmidt, Christoph Schwanke, Daniel Lockau, Sonya Calnan, Tim Frijnts, Sebastian Neubert, Andreas Schöpke, Frank Schmidt, Jens-Hendrik Zollondz, Andreas Heidelberg, Bernd Stannowski, Bernd Rech, and Rutger Schlatmann

***Abstract*—The influence of the transparent conducting oxide (TCO) topography was studied on the performance of a silicon oxide intermediate reflector layer (IRL) in a-Si/μc-Si tandem cells, both experimentally and by 3-D optical simulations. Therefore, cells with varying IRL thickness were deposited on three different types of TCOs. Clear differences were observed regarding the performance of the IRL as well as its ideal thickness, both experimentally and in the simulations. Optical modeling suggests that a small autocorrelation length is essential for a good performance. Design rules for both the TCO topography and the IRL thickness can be derived from this interplay.**

***Index Terms*—3-D rigorous optical modeling, a-Si/μc-Si, intermediate reflector, micromorph, solar cells, transparent conducting oxide (TCO).**

I. Introduction and Background

As THE demand for affordable clean energy grows, amorphous silicon (a-Si) / microcrystalline silicon (μc-Si) tandem solar cells are an interesting technology, as it combines nontoxic and abundant materials with a low temperature/low cost process. However, the conversion efficiency of these devices, which is as high as 12% on lab scale [1], is low compared with other approaches. It is agreed that one of the main limitations of this technology is the limited current provided by the a-Si top cell. Here, a tradeoff regarding the thickness has to be made between 1) high currents and 2) good electronic properties and stability against light-induced degradation. This limits the ideal thickness of the top cell to typically around 200–300 nm. As both subcells are connected in series, this also limits the total current of the tandem device. Prominent strategies to increase the current in the top cell without increasing its thickness, thus circumventing the mentioned tradeoff, are textured transparent conducting oxides (TCOs)—enhancing the optical path through the device—and intermediate reflector layers (IRLs) deposited between the top and the bottom cell [2], [3]. In the superstrate configuration discussed here, the textured TCO acts as a light scatterer, a substrate for the growing film, and as the front electrode. It is known that the different textures obtained—depending on the TCO type and the process conditions—have a significant influence on the amount of light absorbed and on the quality of the absorber layer grown on top of it [4]. Because of differences in the absorption behavior, ideal topographies differ for cells made of a-Si and μc-Si [5].

With respect to the IRL, it was previously found experimentally that the roughness of the TCO also has an influence on the performance of the IRL. As its optical thickness is of the same order of magnitude as the wavelengths that are to be reflected, interference- and near-field effects have to be considered: for a planar system, the variation of the intermediate reflector layer thickness (t_{IRL}) leads to oscillations in the implied photocurrent density of reflectance, which increase in amplitude with increasing light scattering as shown in [6]. The maximum of the first oscillation is the ideal t_{IRL} in case of the top cell limitation. The calculation of the change in ideal t_{IRL} and the maximum gain in the top cell current depending on the TCO topography is one main topic of this publication. It was previously found that the description of the IRL is not sufficiently accurate using 1-D optical models that are based on the tracing of the light [7]. Using a more computationally intensive wave optic theory, it was found that not only the amplitude but also the period (and therewith the ideal t_{IRL}) of the oscillation increases with improved light scattering [8], [9]. This can be explained by the fact that the component of the wave vector going into normal

Manuscript received June 16, 2013; revised August 3, 2013; accepted August 13, 2013. This work was supported in part by the Federal Ministry of Education and Research, the Federal Ministry of environment, and the state government of Berlin in the framework of the program "Spitzenforschung und Innovation in den Neuen Ländern" under Grant 03IS2151 and the Demo14 project under Grant 0325237.

S. Kirner, C. Schwanke, S. Calnan, S. Neubert, A. Schöpke, B. Stannowski, B. Rech, and R. Schlatmann are with Helmholtz-Zentrum Berlin, Berlin 14109, Germany (e-mail: simon.kirner@helmholtz-berlin.de; cmsa@gmx.de; sonya.calnan@helmholtz-berlin.de; Sebastian.neubert@helmholtz-berlin.de; schoepke@helmholtz-berlin.de; bernd.stannowski@helmholtz-berlin.de; bernd.rech@helmholtz-berlin.de; rutger.schlatmann@helmholtz-berlin.de).

M. Hammerschmidt and F. Schmidt are with Konrad-Zuse-Zentrum für Informationstechnik Berlin, Berlin 10717, Germany (e-mail: hammerschmidt@zib.de; frank.schmidt@zib.de).

D. Lockau is with Helmholtz-Zentrum Berlin, Berlin 14109, Germany, and also with Konrad-Zuse-Zentrum für Informationstechnik Berlin, Berlin 10717, Germany (e-mail: daniel.lockau@helmholtz-berlin.de)

T. Frijnts, J.-H. Zollondz, and A. Heidelberg are with Masdar PV GmbH, Ichtershausen 99334, Germany (e-mail: tfrijnts@masdarpv.com; hzollondz@masdarpv.com; aheidelberg@masdarpv.com).

Color versions of one or more of the figures in this paper are available online at http://ieeexplore.ieee.org.

Digital Object Identifier 10.1109/JPHOTOV.2013.2279204

direction, which sets the resonance condition, is reduced with increasing light scattering.

To investigate this interplay systematically, we analyzed a-Si/μc-Si tandem solar cells with varying t_{IRL} on three different TCOs commonly used in thin-film silicon solar cells (SnO_2:F, ZnO:Al, and ZnO:B). The experiments were accompanied by rigorous optical simulations for three wavelengths (600, 650, and 700 nm) and qualitatively good agreement was obtained. As expected, significant differences in the performance of the IRL depending on the topography of the TCO were found.

Through the synthetization of topographies, we were able to analyze the influence of two important characteristics of the topography, independently. By varying the autocorrelation length (ACL) of the synthesized topographies for different root mean square values of the height distribution (RMS), the differences regarding the IRL performance can be explained.

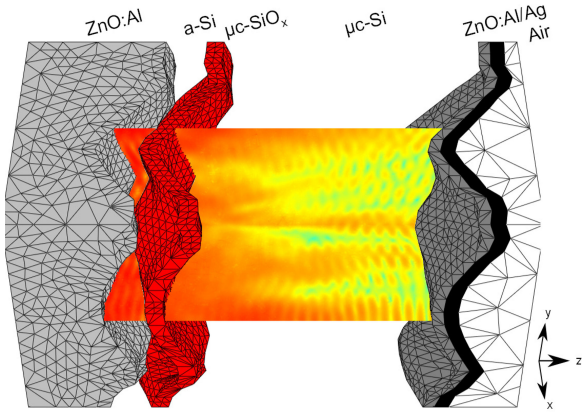

Fig. 1. Example of a 3-D model of an a-Si/μc-Si tandem cell generated based on the measured topography of ZnO:Al TCO. The silicon absorber layers are not shown. The electric field intensity is shown as a false-color plot on a logarithmic scale.

II. Experimental and Simulation Details

The TCOs were in all cases deposited and optimized for large area application in solar cells by external partners. The SnO_2:F was deposited by atmospheric pressure chemical vapor deposition, the ZnO:B by low pressure chemical vapor deposition and the ZnO:Al by means of dc sputtering. The texture etching of the ZnO:Al layers was performed before the solar cell deposition using HCl [10]. The solar cells were deposited in an industrial-like AKT-1600 PECVD multichamber system using an excitation frequency of 13.56 MHz on a substrate size of 30 cm $\times$ 30 cm with 3-mm glass thickness. Because of reasons described, i.e., in [11], we adjusted the p-layer to the TCO to assure a low ohmic contact resistance. The top- and bottom-cell i-layers have a nominal thickness of 290 and 1800 nm, respectively. The IRL consists of μc-SiO_x and is placed in between two 5–10 nm μc-Si n-layers [12]. The thickness of the IRL (t_{IRL}) was varied between 0 and 150 nm. For the sample where t_{IRL} is zero, the n-layer consisted of 30-nm n-μc-Si. A TCO/Ag stack was used as a back contact and reflector. The cells were structured by means of a laser into a size of 1 cm $\times$ 1 cm.

The topography and light scattering properties of the TCOs were characterized using atomic force microscopy (AFM), Haze measurements using a Perkin–Elmer Lambda 1050 UV–Vis-NIR photospectrometer with an integrating sphere, and angular resolved transmission measurements. The solar cells were characterized using a dual source sun simulator (Wacom WXS-155S-L2, class AAA). A differential spectral response setup was used to measure the external quantum efficiency (EQE). To reduce the contribution of the field dependence on the collection efficiency, a high reverse bias voltage of –1.5 V was applied during the EQE measurements. In this way, differences between the devices that originate from the different material qualities obtained on the varying TCOs could be minimized. In addition, the comparison with the simulation, where perfect collection efficiency is assumed, is more reasonable this way. The total reflection measurements were performed using a spectrophotometer.

The finite-element method was used to compute a solution to Maxwell's equations in 3-D in order to determine the EQE of the studied solar cell geometries. The employed simulator is based on JCMsuite by JCMwave [13] and an analysis of the numerical accuracy to the simulator can be found in [14]. The different cells were modeled as axis-aligned periodic unit cells based on the AFM scans of the investigated TCOs (cf., Fig. 1). The AFM scans were cut into smaller samples of 1.8 μm $\times$ 1.8 μm size and mirrored along x- and y-axes, creating periodic samples, which are manageable in domain size and previously were shown to yield a good agreement with experimental results [15]. Aside from a planar interface between the glass half-space and the TCO, the same measured topography was applied for all material interfaces throughout the cell layer stack. This assumption of conformal growth is a simplification of the actual cell geometry as layer growth is not purely directional with the employed deposition methods. However, for the wavelengths analyzed here (600, 650, 700 nm) the topology of the back reflector is of minor interest, as light of these wavelengths, scattered at the back reflector, will be absorbed in the bottom cell i-layer independently of its scattering direction. The vertical layer stack in illumination direction consists of: glass half-space/TCO/a-Si/IRL/μc-Si/ZnO:Al/Ag/Air half-space with nominally the same thicknesses as in the experiment. The optical constants of the IRL were measured experimentally from a single layer on the glass, by fitting transmission and reflection measurements to the Tauc–Lorentz dispersion model. For the other layers, datasets given in the literature were used [16], [17]. In order to keep computation times reasonable, the doped layers (except for the IRL itself) were not considered in our computational cell model.

In $\pm z$-directions of the finite-element domain, adaptive perfectly matched layers [18] are used as boundary conditions to ensure transparency of the domain in these directions. Because of the mirror symmetric construction of the unit cell only one quarter of it needs to be discretized if appropriate mirror boundary conditions are applied laterally and if the incident field has the same symmetry. As illuminating light source, we used a plane wave in normal incidence with respect to the solar cell stack and with a polarization that matches the applied lateral

boundary conditions. The initial reflection of the air/glass interface was calculated analytically using Fresnel's equations.

To synthesize randomly textured topographies with a given circular autocorrelation function (ACF), a method described in [19] and [20] was used. Using the inverse Fourier transform of the amplitude power spectral density (APSD) with randomized phases allows the generation of topographies with specific, parameterized ACFs like the following expression:

$$\mathrm{ACF}(d) = \mathrm{RMS}^2 \cdot \exp\left(\frac{3}{2}\left(\frac{d}{(\mathrm{ACL})}\right)^2\right) \qquad (1)$$

where d is the distance from the origin. The APSD can be derived from the Fourier transform of the ACF. It should be mentioned that the synthesized random topologies reproduce the given ACFs well; however, the angular distributions might be different. Each cell simulation was executed using ∼5 million degrees of freedom. The simulation results for each cell configuration were averaged over at least six AFM samples or synthesized samples amounting to a large number of overall simulations, hence, the restriction to a small wavelength selection.

III. Results and Discussion

In Fig. 2, the AFM scans of the TCOs are shown together with the two characteristic values RMS and ACL. The ACL gives information about the lateral size distribution of the features and can easily be calculated from the AFM data using the appropriate software. The three types of TCO were also analyzed regarding their electrical properties (carrier density and mobility) as well as their transmittance. The results of these studies are not discussed here, as they do not affect the performance of the IRL directly. The analyzed TCOs have been compared in detail before [21] and it is generally agreed upon that due to the large features obtained by etching, the ZnO:Al films yield high bottom cell (>15 mA/cm^2) and total currents (>29 mA/cm^2) in a-Si/μc-Si tandem solar cells. This is due to a superior light trapping of the long wavelength region, which is in agreement with theoretical predictions [5]. On the other hand, the highest top cell currents (>14 mA/cm^2) reported are usually obtained on ZnO:B [22] or SnO_2:F [23], which is generally ascribed to the fact that the features of these TCOs have steeper angles, which scatter the relevant light into wider angles [21]. As can be seen in Fig. 3, our solar cell results are in line with these previously reported observations. It should be mentioned that the use of textured glass substrates, which are not considered here, has led to further improvements in the total photocurrent density in a-Si/μc-Si tandem cells [1], [24] and μc-Si single junction cells [25]–[27], recently.

The TCOs were furthermore characterized using haze–and angular resolved scattering (ARS) measurements. These techniques give direct information about the scattering properties of a given topography against air. In the bottom part of Fig. 2, it can be seen that the ZnO:Al outperforms the other two TCOs in terms of light scattering. However, regarding the application in solar cells, it has previously been found that these characteristics do not necessarily correlate with the implied photocurrent

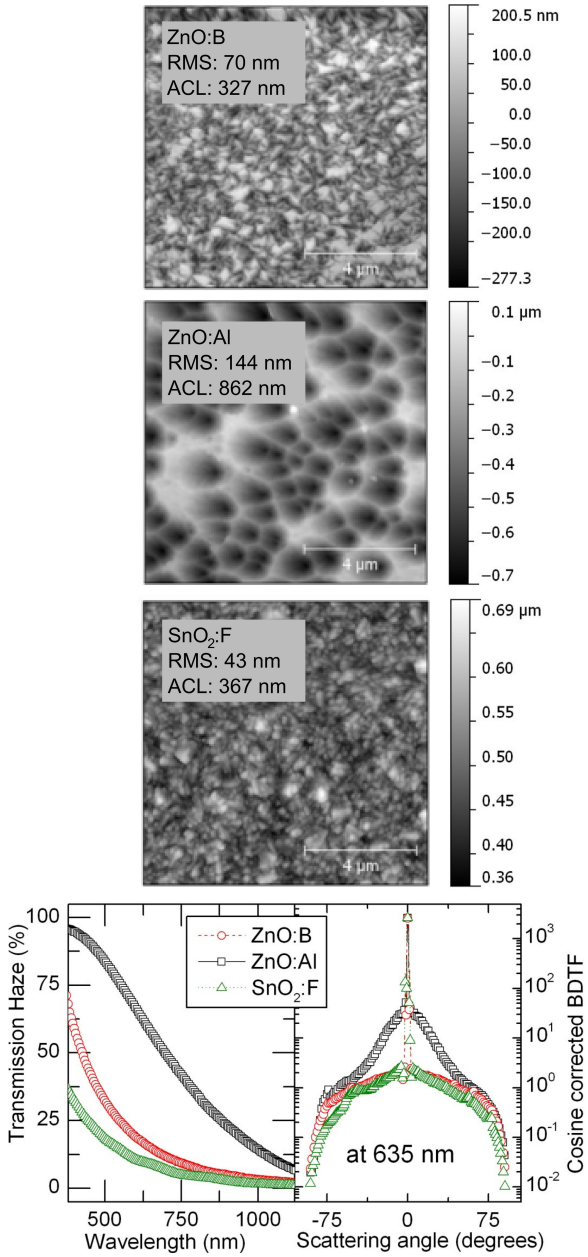

Fig. 2. (Top) AFM scans with the two characteristics, RMS and ACL, and (bottom left) the transmission haze characteristics as a function of wavelength and (bottom right) the cosine corrected bidirectional transmission function (BDTF), as obtained from ARS measurements, of the three analyzed TCOs.

density of the absorbed light in the absorber layers due to the differences in the interface properties. This is in particular the case for the short wavelengths region, and thus, for the top cell [21]. With respect to the intermediate reflector performance studied in this paper and presented in Figs. 3–5, it was found that neither quantitative nor qualitative correlation was found to these optical characteristics. In Fig. 3, three examples of the experimentally obtained quantum efficiencies are depicted of devices deposited on the different TCOs with t_{IRL} of 0, 60, and 120 nm. As can be seen by the magnitude of the current densities, the light in-coupling varies significantly on the different TCOs, i.e., the total current varies between 21.5 and 24.2 mA/cm^2, for t_{IRL}

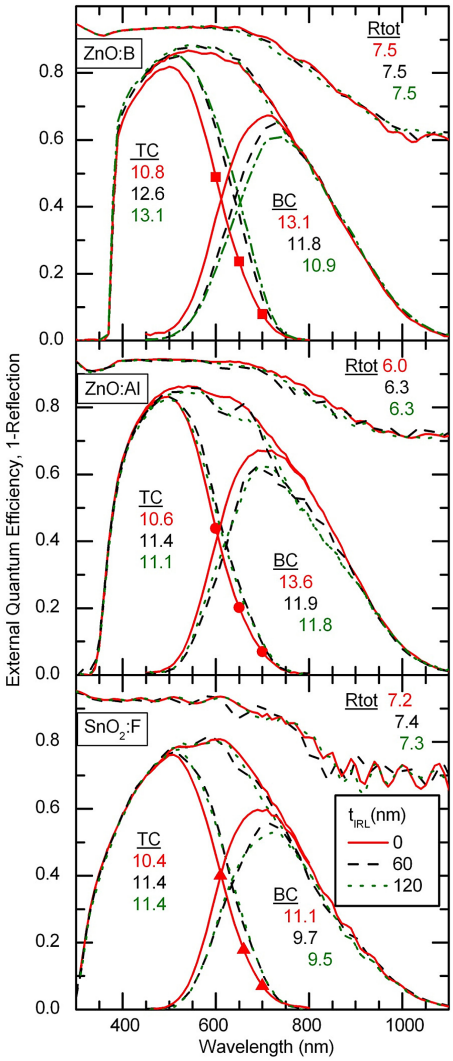

Fig. 3. EQE and total absorptance $(1 - R)$ as a function of wavelength for selected tandem solar cells deposited on the three different TCOs. The numbers indicate the implied photocurrent densities (in mA/cm^2) for the subcells as well as the amount of implied photocurrent of total reflectance (R_{tot}). Some EQE values for the wavelengths, which were also used in the simulation (600, 650, and 700 nm) and are shown in Fig. 5, are marked by symbols.

$= 0$ nm, which can be mainly attributed to the differences in light scattering and the differences in the transmittance of the TCO and the top cell p-layer. In addition, the IRL performance, which shall be defined here as the gain in top cell current density compared with the current density obtained without an IRL ($t_{\mathrm{IRL}} = 0$ nm), is significantly different. The highest gain is obtained on the ZnO:B with 2.3 mA/cm^2 at $t_{\mathrm{IRL}} = 120$ nm, which is still below values reported elsewhere [28]. On the other two TCOs, the maximum gain is significantly less and at lower t_{IRL}s. With respect to the total absorptance $(1 - R)$, one can observe that no current is lost with increasing t_{IRL} on the ZnO:B, on the other hand, increasing total reflection can be observed on the SnO_2:F and the ZnO:Al, similar to observations reported in [7]. However, the increase in total reflection cannot explain the entire loss in the total absorbed current. It is, thus, believed that parasitic absorption increases significantly, presumably, through

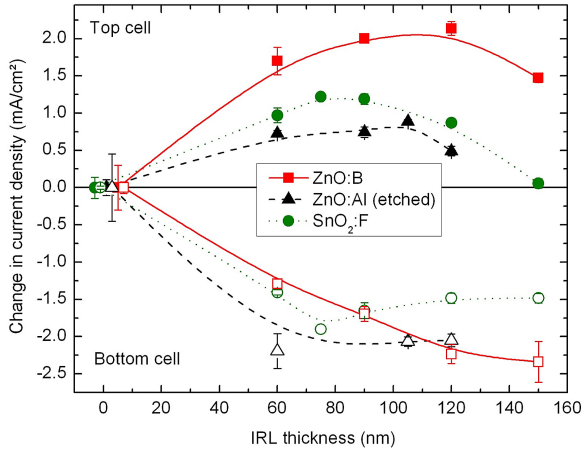

Fig. 4. Experimentally obtained changes in current density in the subcells as obtained by EQE of devices with IRL with indicated thickness compared with devices without IRL. The symbols and error bars indicate the mean and standard deviation of different cells of the same runs. Lines are guides to the eye.

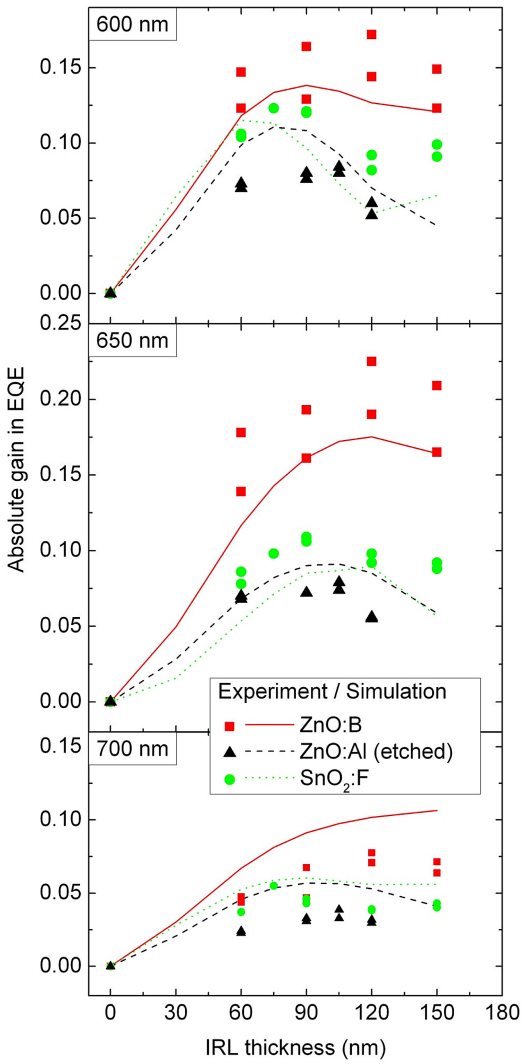

Fig. 5. Experimentally obtained values (symbols) and simulation results (lines) of the gain in top cell EQE at 600, 650, and 700 nm as a function of IRL thickness for the three analyzed TCOs.

reflected light being trapped inside the front TCO [29]. It can be summarized that experimentally, a significant dependence of the IRL performance and ideal t_{IRL} on the type of TCO was observed.

To study the interplay between the IRL performance and the TCO topography in more detail and to gain a better understanding of how the topography affects the performance of the IRL, optical calculations were performed. Therefore, the same variations of t_{IRL} were performed in the simplified layer stacks based on the AFM scans described earlier. Because of the high computation time, the EQE was calculated so far only for three wavelengths (600, 650, and 700 nm), and thus, no integrated current density can be shown. Fig. 5 shows the absolute gain in top cell EQE [i.e., EQE(t_{IRL}=x)–EQE(t_{IRL} = 0 nm)] for the calculated (lines) and the experimentally measured values for two different cells of the same run (as symbols) at the three wavelengths as a function of IRL thickness for the different TCOs. The discrepancy between the two experimentally observed values stems from the spatial inhomogeneity of the top cell i-layer thickness. When looking at the trend of the absolute gain in EQE, one can observe the first maximum of Fabry–Perot oscillations, which occur like on flat interfaces (cf., [6]) despite the roughness of the TCO.

Comparing experiment and simulation, there are rather high discrepancies between the absolute values. Reasons for this can be, for example, differences in the top cell i-layer thickness, which is known to be a function of substrate roughness, imprecisions in the AFM scans and differences in the growth of the IRL and resultant differences in the optical constants, which are all not considered in the simulation. Despite these divergences, one can observe important qualitative parallels between experiment and simulation. First, in both cases, the gain in EQE is the highest on ZnO:B. The other two analyzed TCOs perform fairly similar both experimentally and within the simulation, despite having a significantly different topography. Second, it can be seen that the maximum of the first oscillation shifts to higher t_{IRL} in the case of ZnO:B. The shift in the ideal t_{IRL} toward higher thicknesses can be explained by the fact that the period of the Fabry–Perot oscillations increases due to the reduction in the z-component of the wave vector due to light scattering, as discussed in the beginning and in [8].Taking the AFM properties of the ZnO:Al and ZnO:B into account and comparing it with the IRL performance, another important conclusion should be drawn. The RMS value is not a solid figure of merit for the performance of the IRL. For example, the highest absolute gain in top cell EQE for ZnO:B (RMS = 70 nm) is $>$2 mA/cm^2, the highest gain on ZnO:Al (RMS = 144 nm) is $<$1 mA/cm^2. More important seems to be the lateral dimension (i.e., the ACL).

To emphasize this and to derive implications regarding an ideal topography for the IRL, synthetic topographies were generated using the previously described method with varying ACLs for two different RMS values of 70 and 144 nm. The top cell current gain of a 60 nm IRL compared with no IRL was calculated at a wavelength of 700 nm. As can be seen in Fig. 6, low ACL values are essential for a good performance, rather than high RMS. The calculations indicate, that the high gain in the top cell current obtained on ZnO:B, can be even increased by a further reduction in the ACL. However, the growth of high quality material becomes presumably more difficult on such topographies as mentioned in the beginning and in [5]. Further wavelengths have to be considered for predictive modeling.

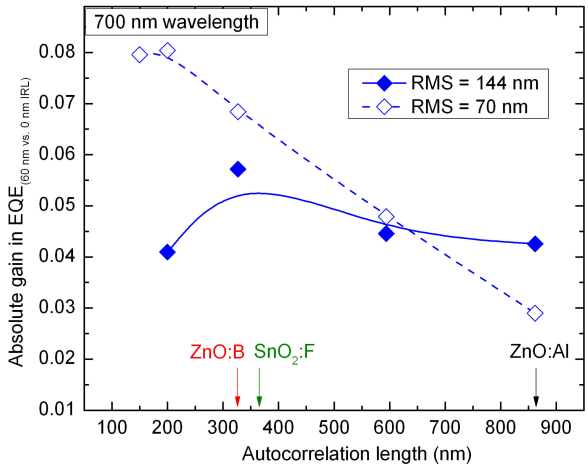

Fig. 6. Simulated gain in top cell current density between 60 and 0 nm IRL at a wavelength of 700 nm as a function of ACL for two different RMS values for synthetically generated topographies. In addition, shown are the experimentally obtained ACL values for the TCOs. Lines are guides to the eye.

IV. Conclusion

We have analyzed the interplay between TCO topography and IRL performance both experimentally and by rigorous optical calculations. Experimentally, we have obtained significantly different IRL performances on the analyzed TCOs: ZnO:B, ZnO:Al, and SnO_2:F. Optical simulations came qualitatively to similar results, which confirm that this is not an experimental artifact. We explain this with the different light scattering properties that lead to significant differences in the ideal IRL design. The difference in the ideal thicknesses can be explained by the reduction of light being reflected in the normal direction and a resulting increase in oscillation period, as predicted by the wave optic theory. The presented approach can be used to calculate improved topographies for high top cell currents.

Acknowledgment

The authors would like to thank M. Zelt and S. Ring for their technical assistance.

References

[1] U. Kroll, J. Meier, L. Fesquet, J. Steinhauser, S. Benagli, J. Orhan, B. Wolf, D. Borrello, L. Castens, Y. Djeridane, X. Multone, G. Choong, D. Domine, J.-F. Boucher, P.-A. Madliger, M. Marmelo, G. Monteduro, B. Dehbozorgi, D. Romang, E. Omnes, M. Chevalley, G. Charitat, A. Pomey, E. Vallat-Sauvain, S. Marjanovic, G. Kohnke, K. Koch, J. Liu, R. Modavis, D. Thelen, S. Vallon, A. Zakharian, and D. Weidman, "Recent developments of high-efficiency micromorph tandem solar cells in Kai-m/plasmabox PECVD reactors," in *Proc. 26th Eur. Photovoltaic Sol. Energy Conf.*, 2011, pp. 2340–2343.

[2] A. Lambertz, T. Grundler, and F. Finger, "Hydrogenated amorphous silicon oxide containing a microcrystalline silicon phase and usage as an intermediate reflector in thin-film silicon solar cells," *J. Appl. Phys.*, vol. 109, pp. 113109-1–113109-11, 2011.

[3] P. Buehlmann, J. Bailat, D. Dominé, A. Billet, F. Meillaud, A. Feltrin, and C. Ballif, "In situ silicon oxide based intermediate reflector for thin-film silicon micromorph solar cells," *Appl. Phys. Lett.*, vol. 91, pp. 143505-1–143505-3, 2007.

[4] M. Python, O. Madani, D. Dominé, F. Meillaud, E. Vallat-Sauvain, and C. Ballif, "Influence of the substrate geometrical parameters on microcrystalline silicon growth for thin-film solar cells," *Sol. Energy Mater. Sol. Cells*, vol. 93, pp. 1714–1720, 2009.

[5] B. Lipovsek, M. Cvek, A. Campa, J. Krc, and M. Topic, "Analysis and optimisation of periodic interface textures in thin-film silicon solar cells," in *Proc. 25th Eur. Photovoltaic Sol. Energy Conf.*, 2010, pp. 3120–3123.

[6] N. P. Vaucher, J.-L. Nagel, R. Platz, D. Fischer, and A. Shah, "Light management in tandem cells by an intermediate reflector layer," in *Proc. 2nd World Conf. Photovoltaic Sol. Energy Convers.*, 1998, pp. 729–731.

[7] D. Dominé, J. Bailat, J. Steinhauser, A. Shah, and C. Ballif, "Micromorph solar cell optimization using a ZnO layer as intermediate reflector," *Photovoltaic Energy Convers.*, vol. 2, pp. 1465–1468, 2006.

[8] C. Rockstuhl, F. Lederer, K. Bittkau, T. Beckers, and R. Carius, F. Lederer, K. Bittkau *et al.*, "The impact of intermediate reflectors on light absorption in tandem solar cells with randomly textured surfaces," *Appl. Phys. Lett.*, vol. 94, pp. 211101-1–211101-3, 2009.

[9] S. Fahr, C. Rockstuhl, and F. Lederer, "The interplay of intermediate reflectors and randomly textured surfaces in tandem solar cells," *Appl. Phys. Lett.*, vol. 97, pp. 173510-1–173510-3, 2010.

[10] J. Müller, B. Rech, J. Springer, and M. Vanecek, "TCO and light trapping in silicon thin film solar cells," *Sol. Energy*, vol. 77, pp. 917–930, 2004.

[11] J. Rath and R. Schropp, "Incorporation of p-type microcrystalline silicon films in amorphous silicon based solar cells in a superstrate structure," *Sol. Energy Mater. Sol. Cells*, vol. 53, pp. 189–203, 1998.

[12] S. Kirner, S. Calnan, O. Gabriel, S. Neubert, M. Zelt, B. Stannowski, B. Rech, and R. Schlatmann, "An improved silicon-oxide-based intermediate-reflector for micromorph solar cells," *Phys. Status Solidi C*, vol. 9, pp. 2145–2148, 2012.

[13] J. Pomplun, S. Burger, L. Zschiedrich, and F. Schmidt, "Adaptive finite element method for simulation of optical nano structures," *Phys. Status Solidi B*, vol. 244, pp. 3419–3434, 2007.

[14] M. Hammerschmidt, D. Lockau, S. Burger, F. Schmidt, C. Schwanke, S. Kirner, S. Calnan, B. Stannowski, and B. Rech, "FEM-based optical modeling of silicon thin-film tandem solar cells with randomly textured interfaces in 3D," *Proc. SPIE*, vol. 8620, pp. 86201H-1–86201H-9, 2013.

[15] C. Jandl, K. Hertel, C. Pflaum, and H. Stiebig, "Simulation of thin-film silicon solar cells with integrated AFM scans for oblique incident waves," in *Proc. 26th Eur. Photovoltaic Sol. Energy Conf.*, 2011, pp. 2663–2666.

[16] J. Springer, A. Poruba, and M. Vanecek, "Improved three-dimensional optical model for thin-film silicon solar cells," *J. Appl. Phys.*, vol. 96, pp. 5329–5337, 2004.

[17] M. Zeman, R. A. C. M. M. van Swaaij, J. W. Metselaar, and R. E. I. Schropp, "Optical modeling of a-Si: H solar cells with rough interfaces: Effect of back contact and interface roughness," *J. Appl. Phys.*, vol. 88, pp. 6436–6443, 2000.

[18] L. Zschiedrich, "Transparent boundary conditions for Maxwell's equations," Ph.D. dissertation, Dept. Math. Comput. Sci., Free Univ. Berlin, Berlin, Germany, 2009.

[19] J.-J. Wu, "Simulation of rough surfaces with FFT," *Tribol. Int.*, vol. 33, no. 1, pp. 47–58, 2000.

[20] D. Lockau, L. Zschiedrich, S. Burger, F. Schmidt, F. Ruske, and B. Rech, "Rigorous optical simulation of light management in crystalline silicon thin film solar cells with rough interface textures," *Proc. SPIE*, vol. 7933, pp. 79330M-1–79330M-10, 2011.

[21] C. Rockstuhl, S. Fahr, K. Bittkau, T. Beckers, R. Carius, F.-J. Haug, T. Söderström, C. Ballif, and F. Lederer, "Comparison and optimization of randomly textured surfaces in thin-film solar cells," *Opt. Exp.*, vol. 18, pp. A335–A341, 2010.

[22] P. Cuony, D. T. L. Alexander, I. Perez-Wurfl, M. Despeisse, G. Bugnon, M. Boccard, T. Söderström, A. Hessler-Wyser, C. Hébert, and C. Ballif, "Silicon filaments in silicon oxide for next-generation photovoltaics," *Adv. Mater.*, vol. 24, pp. 1182–1186, 2012.

[23] V. Smirnov, A. Lambertz, B. Grootoonk, R. Carius, and F. Finger, "Microcrystalline silicon oxide alloys: A versatile material for application in thin film silicon single and tandem junction solar cells," *J. Non-Cryst. Solids*, vol. 358, pp. 1954–1957, 2012.

[24] M. Boccard, C. Battaglia, S. Hänni, K. Söderström, J. Escarr, S. Nicolay, F. Meillaud, M. Despeisse, and C. Ballif, "Multiscale transparent electrode architecture for efficient light management and carrier collection in solar cells," *Nano Lett.*, vol. 12, pp. 1344–1348, 2012.

[25] H. Sai, K. Saito, N. Hozuki, and M. Kondo, "Enhanced photocurrent and conversion efficiency in thin-film microcrystalline silicon solar cells using periodically textured back reflectors with hexagonal dimple arrays," *Appl. Phys. Lett.*, vol. 101, pp. 173901-1–173901-5, 2012.

[26] O. Isabella, F. Moll, J. Krc, and M. Zeman, "Modulated surface textures using zinc-oxide films for solar cells applications," *Phys. Status Solidi A*, vol. 207, no. 3, pp. 642–646, 2010.

[27] P. I. Widenborg and A. G. Aberle, "Polycrystalline silicon thin-film solar cells on AIT-textured glass superstrates," *Adv. Opto. Electron.*, vol. 2007, pp. 1–7, 2007.

[28] D. Dominé, P. Buehlmann, J. Bailat, A. Billet, A. Feltrin, and C. Ballif, "Optical management in high-efficiency thin-film silicon micromorph solar cells with a silicon oxide based intermediate reflector," *Phys. Status Solidi, RRL*, vol. 2, no. 4, pp. 163–165, 2008.

[29] F.-J. Haug, K. Söderstrom, A. Naqavi, and C. Ballif, "Resonances and absorption enhancement in thin film silicon solar cells with periodic interface texture," *J. Appl. Phys.*, vol. 109, pp. 084516-1–084516-8, 2011.

Author's photographs and biographies not available at the time of publication.